Bollettino di Geofisica Teorica ed Applicata Vol. 61, n. 2, pp. 119-130; June 2020
DOI 10.4430/bgta0307

Shallow shear-wave velocity structure by short period ambient noise Rayleigh wave phase velocities from beamforming and cross-correlation techniques in north-eastern Iran

S.M. Azhari[1], M. Rezapour[1] and A.A. Mottaghi[2]

[1] *Institute of Geophysics, University of Tehran, Iran*
[2] *University of Urmia, Tehran, Iran*

(Received: 22 August 2019; accepted: 5 November 2019)

ABSTRACT We derived an average shallow shear-wave velocity model for the metropolitan Mashhad city and surrounding region in north-eastern Iran based on ambient noise Rayleigh waves dispersion curves. Phase velocity dispersions, for comparison, came from both beamforming analysis in the frequency domain as finding the average phase velocity within the array, and the spectral method of Bessell function estimations directly from Fourier transform of noise correlation functions provided in the time domain between individual station pairs of known distances across the array. Our results showed a strong agreement between two dispersion measurements. Finally, we inverted the average phase velocity dispersion curves obtained from both the beamforming and Bessel function techniques. Finally, the neighbourhood algorithm was adopted to provide an average 1D shear-wave velocity model.

Key words: velocity structure, ambient noise, beamforming, cross-correlation, NE Iran.

1. Introduction

The disastrous impacts of the 5 April 2017 moderate earthquake with magnitude M_W 6.0 in the vicinity of the metropolitan Mashhad city in north-eastern Iran, together with the history of significant seismic activity, emphasise the importance of early warning system and risk mitigation programs in this region. On the other hand, the city of Mashhad is under a significant seismic hazard because its proximity to the Kashafrud and Binalud fault systems (Fig. 1). One of the key parameters, especially for the study of the influence of local geologic and shallow sub-surface structures on the intensity of ground shaking, is the shear-wave velocity structure. The effect of strong near-field motion, including abnormal strong ground motion, fault displacement, landslides, liquefaction, amplification of surface waves, and associated health problems are commonly mentioned as likely effects of active faulting in the urban areas (Bostenaru Dan *et al*., 2014). Among these, amplification of surface waves by shallow low velocity structures seems to have been responsible for severe property damage (German and Beroza, 2008).

The foremost tool in shallow velocity studies may be considered as ambient seismic noise. The cross-correlation of ambient seismic noise for pairs of stations has been proven to be an established method for determining interstation surface-wave velocities as well as shear-wave velocity models (e.g. Shapiro *et al*., 2005; Li *et al*., 2009). Thus, given the availability of continuous records, it is

of primary interest to use ambient noise surface waves, mainly because of limitations in frequency ranges of earthquake sources. On the other hand, while group velocities can be unambiguously retrieved from noise cross-correlation functions (Shapiro and Campillo, 2004), phase velocities are not estimated in a straightforward way (Gouedard *et al*., 2008; Harmon *et al*., 2008). For this reason, we made recourse to two independent techniques of phase velocity estimations in the time and frequency domains to obtain average shear-wave velocity structure of the region at shallow depths.

To summarise, the objective of this study is to use continuous data recorded by temporary seismic stations to investigate an average phase velocity dispersion and shear-wave velocity model beneath the city of Mashhad and surrounding region. Phase velocity dispersions, for comparison, come from both beamforming analysis in the frequency domain and correlation functions provided in the time domain.

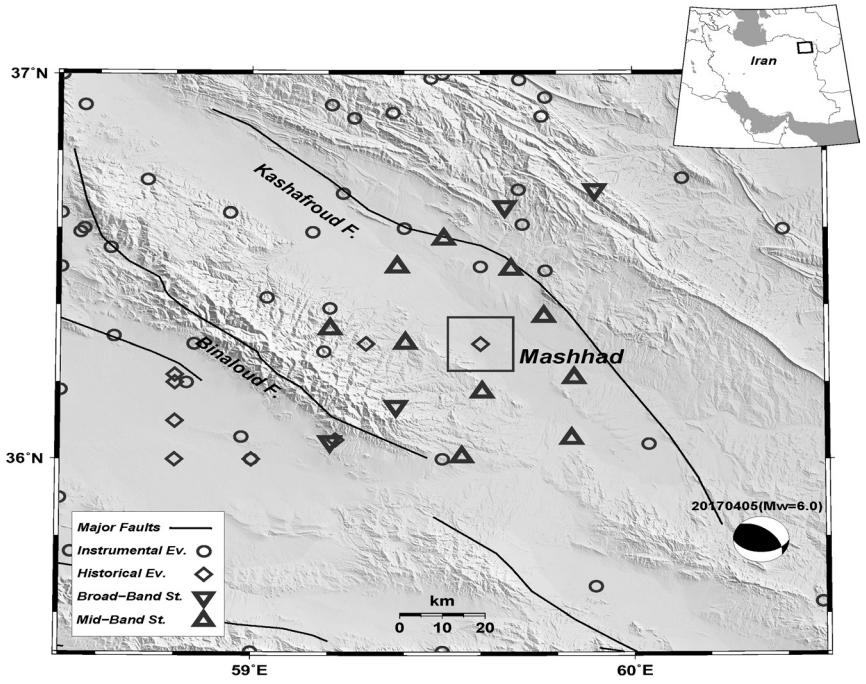

Fig. 1 - Map of the study area. The box indicates the metropolitan Mashhad city in NE Iran and triangles denote seismic stations. Diamonds and circles represent historical and instrumental seismic events with magnitudes larger than 6 and 4, respectively. The beach-ball denotes the 5 April 2017 mainshock occurred on the Kashafroud fault.

2. Tectonic setting of the study area

The Iranian Plateau involves different styles of deformation in various parts, according to the northward motion of the Arabian Shield relative to Eurasia (e.g. Vernant *et al*., 2004). The deformation in NE Iran is concentrated in the Kopeh Dagh seismotectonic province including the Kashafrud and Binalud fault systems (Fig. 1). This deformation is accommodated by crustal shortening and strike-slip faulting in different intracontinental deformation domains in NE Iran.

According to the available geodetic (Vernant *et al*., 2004; Masson *et al*., 2007; Tavakoli, 2007) and geological (Shabanian *et al*., 2009) data, shortening in NE Iran took place at a rate ranging from 4 to 11 mm/a. In the Binalud Mountains, the GPS-derived velocity vectors (Masson *et al*., 2007; Tavakoli, 2007) indicate 2-4 mm/yr of right-lateral strike-slip movement. This region is also a linear intracontinental mountain range that represents the north-eastern suture between the Iranian plateau and Eurasia (Alavi, 1992) including 10-17 km thick, Mesozoic and Tertiary sediments, which were folded during the Oligo-Miocene orogenic movements (Stocklin, 1968; Lyberis and Manby, 1999). Mesozoic and Tertiary sediments of the Kopeh Dagh were folded into parallel, asymmetric NW trending folds during the Oligo-Miocene orogenic movements (Stocklin, 1968; Lyberis and Manby, 1999). These folds are obliquely dissected by strike-slip fault systems that consist of active NNW-trending right-lateral and ENE-trending left-lateral strike-slip faults (e.g. Tchalenko, 1975; Shabanian *et al*., 2009) extended within the western and central Kopeh Dagh. The available very near-surface information indicate that this region is a longitudinal asymmetrical valley filled by the alternation of gravel, sand, silt, and clay materials, and presence of thick alluvial deposits is documented in recent researches (Hafezi Moghaddas, 2008; Sajadian *et al*., 2015). Despite the lack of clear structural linkage between the Kopeh Dagh and Binalud Mountains ranges, the pioneer work by Tchalenko (1975) suggested a possible connection between the two deformation domains. On the other hand, the GPS-derived rate of 2-4 mm/yr for range parallel displacement through the Binalud Mountains (Masson *et al*., 2007; Tavakoli, 2007) implies significant right-lateral strike-slip faulting along both sides of the mountains.

The relationship between seismicity and faulting in this region has recently re-evaluated by Hollingsworth *et al*. (2006) for modern large earthquakes. Since the 19th century, the Kopeh Dagh region has experienced many catastrophic earthquakes and at least nine large earthquakes ($M \geq 7$) during the last six centuries occurred in the vicinity of the Kashafrud and Binalud fault systems (Tchalenko, 1975; Ambraseys and Melville, 1982; Jackson *et al*., 2002).

3. Data

Our data come from a temporary seismic network with a collaborative experiment between the International Institute of Earthquake Engineering and Seismology (IIEES), Tehran, and Cambridge University in the UK.

We analysed continuous data recorded during this temporary seismic survey and at the vertical component of ten mid-band and four broad-band stations (Fig. 1). The time interval for the raw data spans 3 months between 1 October 2006 and 31 May 2007. Our mid-band and broad-band sensors are CMG-6TD and CMG-3T Guralp System sensors, respectively. The data were continuously sampled at 100 samples per second and stamped with GPS time.

4. Phase velocities from beamforming analysis

The beamforming method finds the best fitting of a plane wave crossing a seismic array with a unique phase slowness and backazimuth. Our adopted method for beamforming analysis is similar to that described by Gerstoft *et al*. (2006). The mean, trend, and instrument response are

first removed from all daily records. Next, we split the data for each day into 10-minute sliding windows with 50% overlsps, which were, then, processed by one-bit normalisation and Fourier transform. The phase response from all stations at each frequency was retained for estimation of cross spectral density matrix and averaged for each 1.5 hour data.

The plane wave response for a given frequency, slowness, and azimuth is simulated by $p\,(w, s, q, r) = \exp\,(i\,w(r\,e)/c)$, where w is frequency, s slowness, q azimuth, and e is the directional cosines of the plane wave and r refers to the coordinates of the stations with respect to the centre of array. The beamforming output is then calculated by:

$$b\,(w, s, q, t) = p^{\mathcal{T}}(w, c, q)\,C\,(w, t)\,p\,(w, c, q) \qquad (1)$$

where $C\,(w, t)$ is the cross spectral density matrix over the array for a time interval t (Gerstoft and Tanimoto, 2007; Harmon *et al*., 2008).

At each frequency, we retained all maximum beamforming outputs corresponding to the combinations of azimuths (0-360°) and slownesses (0.2-5.0 s/km) for each 1.5 hour data. The beamforming outputs were, then, normalised relative to the maximum beamforming output of individual day. We repeated the above-mentioned steps for all daily data. Finally, all daily beamforming outputs were stacked and normalised over 2 degrees azimuths. The estimated outputs were transformed to an image by an interpolation technique. To estimate the average phase velocity dispersion curve, we used the maximum beamforming outputs over 2 degrees azimuths as the weights for calculating averages at different frequencies. We also made synthetic tests by analysing some combination of slownesses and frequencies to give an insight into the array response. The tests over frequencies 0.1-1.0 Hz showed that our beamforming analysis is more reliable over the frequency range of 0.1 to 0.3 Hz. Examples of the beamforming outputs at three frequencies, and a typical array response for a plane wave with frequency of 0.2 Hz and back azimuth of 225 degrees are shown in Fig. 2. For the best-resolved frequency range (0.1-0.3 Hz), there are roughly continuous rings of maximum beamforming outputs which correspond to energy coming from various azimuths. Detectable coherent signals extracted from noise cross-correlations are highly dependent on the direction and the frequency content of noise sources (Sabra *et al*., 2005; Gerstoft *et al*., 2006; Stehly *et al*., 2006; Yao and van der Hilst, 2009). The beamforming outputs show that the azimuthal distribution of ambient noise energy is relatively homogenous implying that average phase velocities are less influenced by directionality of noise sources. The average phase velocities are in the range of 1.1 to 2.9 km/s for the frequency range of 0.1 to 0.3 Hz and azimuthal distribution of detectable energy is relatively homogenous.

5. Phase velocities from cross-correlation technique

Continuous data from the vertical component of all station pairs were cross-correlated and stacked to construct empirical Green's functions between stations. The method of data processing is the same that now widely adopted as time domain correlations of Bensen *et al*. (2007). The mean, trend, and instrument response were first removed and decimated to interested frequency range (0.1-5.0 Hz) using an antialiasing filter: then, all data associated with station pairs were cross-correlated for each 30 minutes data. To account for the effect of earthquake signals and

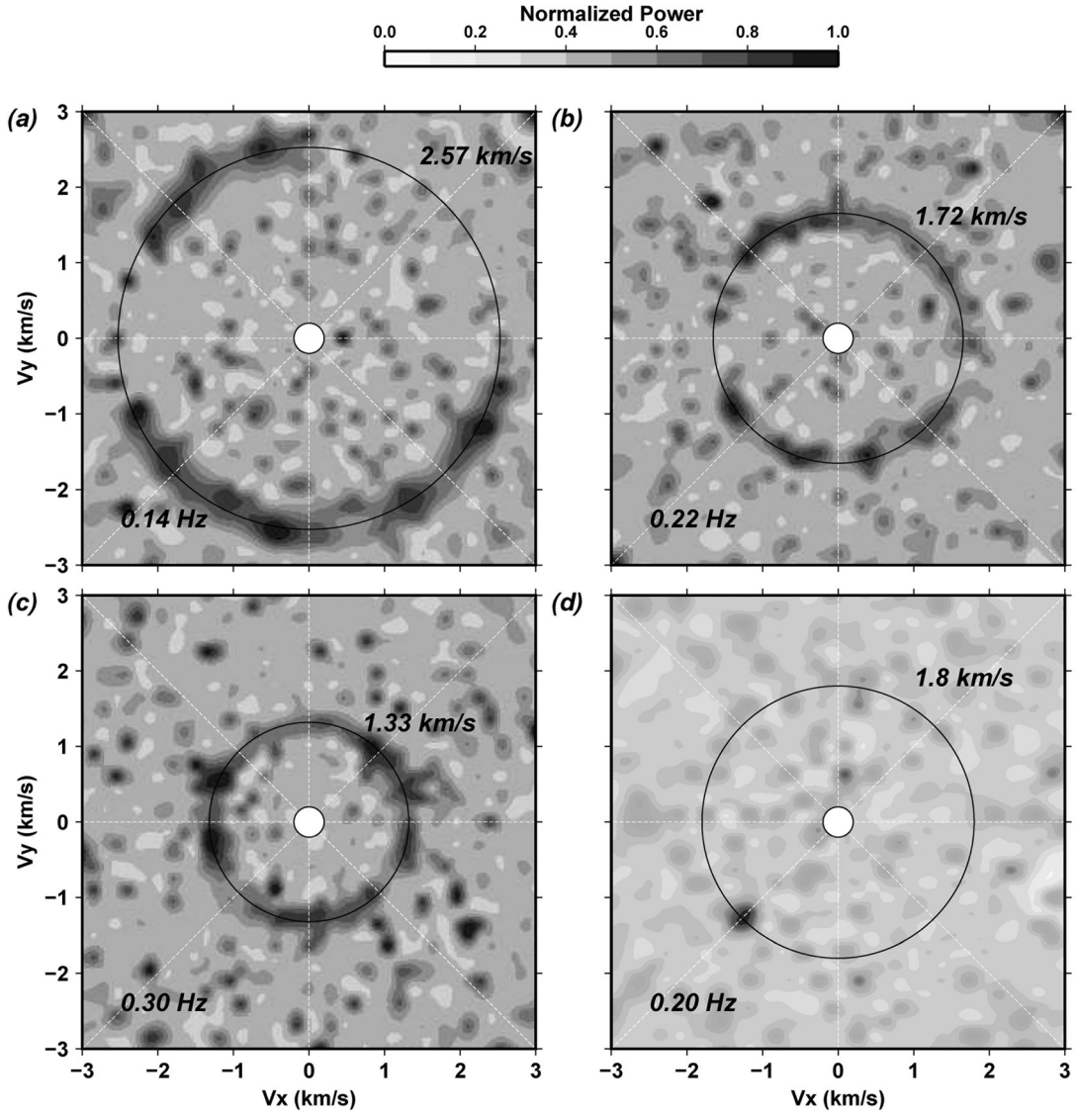

Fig. 2 - Beamforming outputs at frequencies: a) 0.14, b) 0.22, and c) 0.30 Hz. The black open circles represent average phase velocity corresponding to the maximum beamforming outputs over all azimuths. d) A typical array response for a plane wave with frequency of 0.2 Hz and back azimuth of 225 degrees.

dynamic range of frequency dependent seismic noise field, the one-bit normalisation and spectral normalisation (whitening) were performed before calculating cross-correlations. Finally, stacks of 30-min cross-correlations were calculated and the causal and acausal parts of correlations were further stacked to construct station pair correlations. We select only 57% of the correlation functions (52 usable station pairs) with the signal-to-noise ratio (SNR) larger than 7. We determine SNR by dividing the power of maximum amplitude in the cross-correlations signal by the power of the last 30 s of the record. Also, the records with inter-station spacing of less than three complete wavelengths were removed through the next step. Fig. 3a shows an example of noise correlation function for the single station pair BOR-NAZ.

It is well known that we can extract group velocity dispersion curve from noise cross-correlations, and phase dispersion measurements can be obtained by integration of group dispersion curves. This approach, however, is not sufficient to identify phase velocity uniquely (Boschi *et al*., 2013). According to Aki (1957), multiplying the frequency spectrum associated with ambient noise signal recorded in short time interval and at two different stations gives the cross-spectrum (spectrum of the cross-correlation signals) of the two simultaneous records. Stacks or averages of short time cross-spectrums is, then, calculated and referred to as coherency. This coherency must coincide with one of the known zeros of the Bessel function. In other words, the basic idea suggests that the azimuthally averaged normalised cross-spectrum between two receivers takes the form of a zero order Bessel function. Actually, the zeroes in an observed spectrum are associated by zeroes of the Bessel function to estimate phase velocity dispersion. The Bessel function of the first kind is related to the phase velocity by $C(\omega_n) = \omega_n r/Z_n$, where $c(\omega_n)$ is the phase velocity at angular frequency ω_n, r is station pair separation, and Z_n is nth zero of the Bessel function (Ekstrom *et al*., 2009). Thus, following the theory presented by Aki (1957) and widely used by a number of investigators (e.g. Ekstrom *et al*., 2009; Prieto *et al*., 2009; Sadeghisorkhani *et al*., 2018), we take advantage of the real part of correlation spectrum to estimate phase velocity dispersions of different station pairs through the array. Since the azimuthally averaged cross-spectrum in frequency domain is equivalent to the Fourier transform of the time domain cross-correlations, we chose to use the locations of zero crossing points on frequency versus real part of correlation spectrum of cross-correlation functions diagram to estimate phase velocity dispersions. Fig.

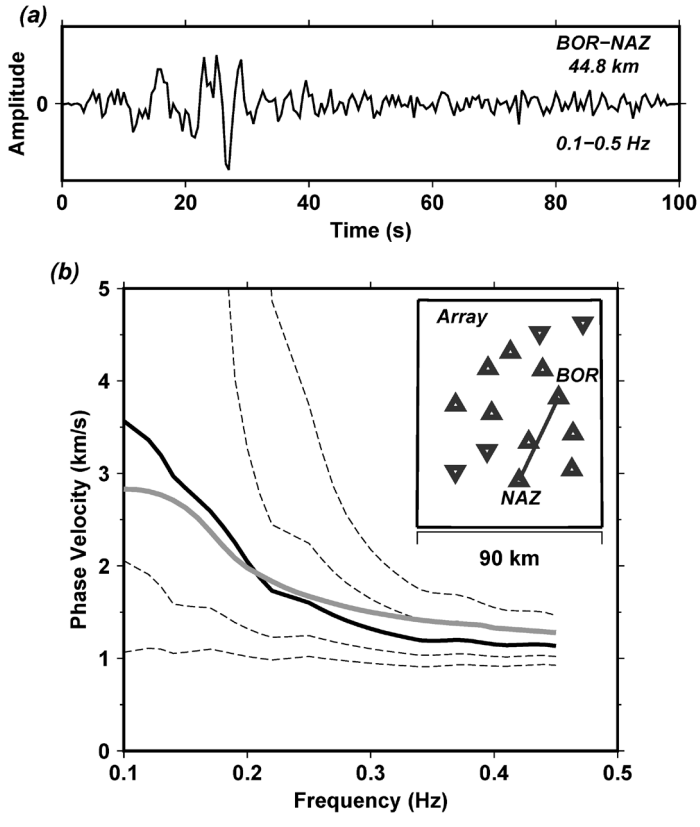

Fig. 3 - An example of noise correlation function (a), and corresponding dispersion measurement by Bessel function technique (b). Information about stations, path, and frequency range is shown on the panels. Solid black line shown on bottom panel corresponds to dispersion curve with no missing or extra zeros crossing points while dashed lines associate additional trial dispersion curves with missing and extra zero crossing points. Gray solid line denotes the average dispersion curve over the array.

3b shows an example of corresponding phase velocity dispersion measurements. According to Ekstrom *et al*. (2009), trial dispersion measurements were also tested using possible association of observed spectra zeros with zero crossing of the Bessel function. Continuity together with the average phase velocities derived from beamforming analysis (previous section) are our criteria for evaluating and selecting proper dispersion curves.

6. Average 1D shear-wave velocity model

Shear-wave velocity can be derived from inverting phase velocity dispersion curve of the surface waves. The Rayleigh wave as prominent surface wave travels along a free surface and is the result of interfering P- and S-waves (Sheriff and Geldart, 1982). For the case of a solid half space, the Rayleigh wave is not dispersive, however, in the case of a one layer over a half space, the Rayleigh wave travels with different wavelengths (or frequencies). The waves with lower frequencies penetrate deeper than those with higher frequencies and sample deeper structures. However, a wide range of different frequencies as a function of surface wave velocities (dispersion curve) can be efficiently used to obtain shear-wave structure of the Earth. On the other hand, model parameters of the true Earth structure affect seismic wave propagation and estimated shear-wave model. In this way, to further assess the effects of model parameters (density, P- and S-wave, and layer's thickness), we investigated a synthetic test based on random changes on model parameters. In this section, we start with creating a dispersion curve for a given Earth model using the method of Herrmann and Ammon (2002). The frequency range is similar to that we extracted from dispersion curves (0.1-1.0 Hz). Fig. 4 indicates our synthetic model and parameters. To accommodate velocity gradients into the model, we introduced five 2-km thick layers over a half space with constant density, P- and S-wave velocity in each layer. In the second step, we randomly perturbed the model parameters more than 100 times, up to 30% in each layer, to evaluate the sensitivity of model parameters on dispersion curve. In summary, for all frequencies, a 30% error in three initial parameters (P-wave velocity, density, and layers thickness) results in maximum 10% difference between the true initial model and dispersion curves (Fig. 4). Fig. 4 demonstrates that inverting phase velocity for layers thickness is relatively sensitive in comparison with P-wave velocity and density parameters. However, average difference between the modelled and actual dispersion curve is still less than those for S-wave velocity. Our analysis shows that the most sensitive parameter on dispersion curve (phase velocities versus frequencies) is S-wave velocity, which is, therefore, the fundamental basis for inverting surface wave phase velocity to Earth model. Thus, we may conclude that inverting a dispersive Rayleigh wave is representative of shear-wave velocity structure of the Earth. In other words, we can only leave S-wave velocity to be unknown for inverting dispersion curve and fix other parameters through the entire process. Actually, S-wave velocities fundamentally control Rayleigh wave velocity distribution in different frequencies for a layered Earth model. As shown in Fig. 4, all three model parameters (P-wave velocity, density, and layers thickness) affect only marginally phase velocities through all frequencies. Changes in S-wave velocities significantly distort the dispersion curve and we must be cautious about this parameter. For this reason, we choose more than 500 randomly distributed initial S-wave velocities between 1 and 4 km/s for each layer.

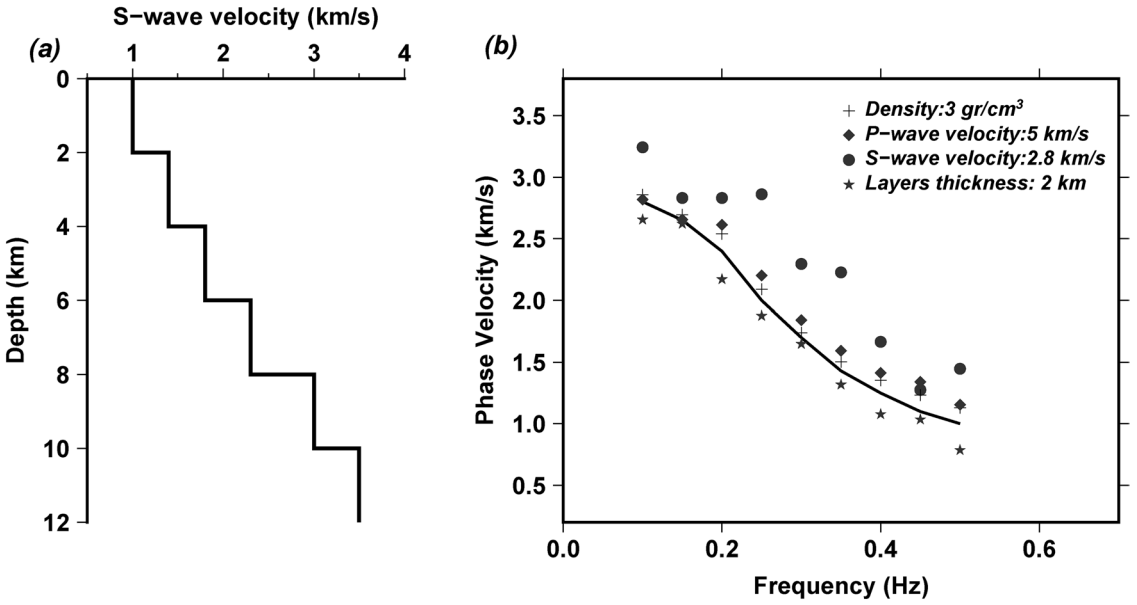

Fig. 4 - An example of synthetic test. Phase velocity distribution by random changes in model parameters: a) assumed Earth model with 2 km thick layers and b) corresponding dispersion curve. The solid line in panel b indicates the dispersion curve corresponding to the given Earth model. Plus symbols, diamonds, circles, and stars represent phase velocities after 30% perturbation in density, P-wave, layers thickness, and S-wave velocity, respectively. Note that S-wave parameter is the most sensitive parameter on velocity changes. Information about average values for parameters are shown in the figure.

Finally, we inverted the average phase velocity dispersion curves obtained from both the beamforming and Bessel function techniques in previous sections using the neighbourhood algorithm provided by Sambridge (1999) and Wathelet (2008). The neighbourhood algorithm is a stochastic direct search method for finding models of acceptable data fit inside a multidimensional parameter space. Given pseudo-random sets of the parameter space for different ground models, the dispersion curves are, then, calculated through a forward problem process and the differences (misfits) between the observed and calculated dispersion curves are compared. Finally, a simple interpolation method is used to find good data-fitting set of parameters which match the final model with the observed dispersion curve.

Our inversion started by applying a simple space parameterisation that accounted for increasing quantised layers until the best fit between the observed and predicted dispersion data is obtained. Our initial models at the last trial inversion (with lowest misfit) is sampled by 6 numbers of 2 km thick layers and the inversion was iterated 500 times. In order to reduce the effect of initial velocity models on the process of inversion, we sampled our 500 initial models by 2 km thick layers in which all velocities were randomly distributed between 1-4 km/s with 0.1 intervals. For each initial model, we obtained a final model with an *rms* value implying the convergence of final solution and stability. In this step, using the accumulated output models we can identify the main interfaces of an average model. The shear-wave models obtained by inversion of the final average dispersion curve is shown in Fig. 5b. The model with minimum misfit value (0.008) corresponds to 0.6-2.2 km/s at 3 km upper layers and 2.2-3.5 km/s at lower layers down to 12 km depth.

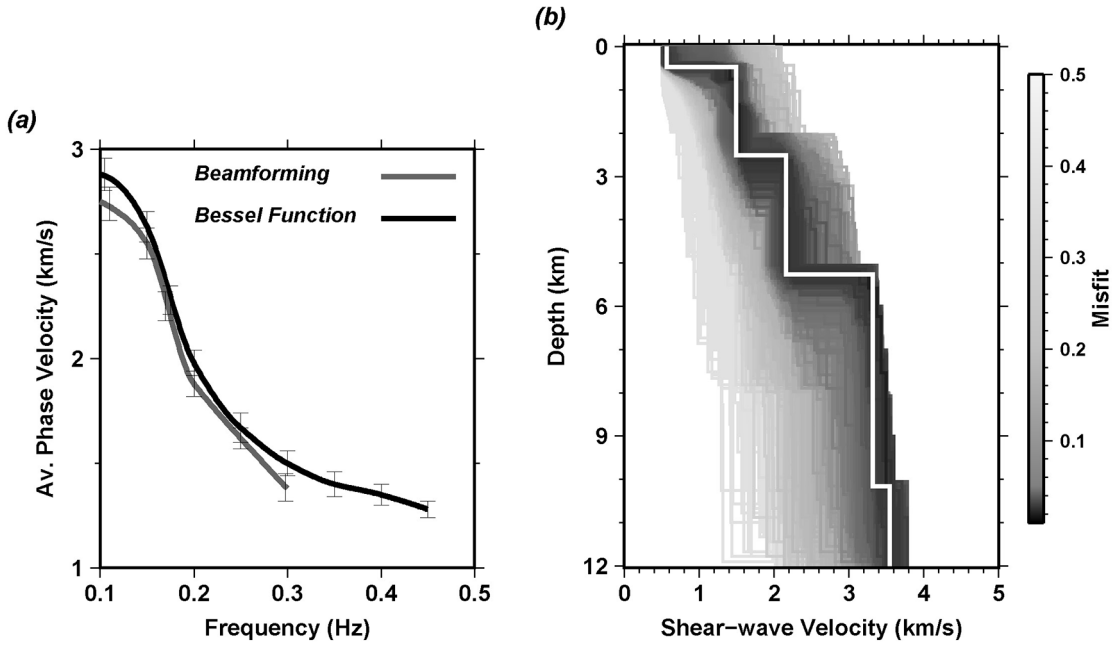

Fig. 5 - a) Average dispersion curves from both beamforming (gray line) and Bessel function (black line) techniques, for some frequencies, two standard deviation ranges are shown by error bars. b) Shear-wave velocity model derived by average dispersion estimates. The inversion was iterated 500 times. White solid line delineates the smoothed model with minimum misfit value.

7. Discussion and conclusions

We derived an average shallow shear-wave velocity model for the city of Mashhad and surrounding region in NE Iran based on ambient noise Rayleigh waves dispersion curves. Two independent techniques of phase velocity dispersion measurements were carried out for comparison and validation.

Array geometry plays an important role in emerging coherent signals of the phase of interests. Depending on various applications, the aperture, station spacing, and number of stations, as the classification parameters of an array, determine the resolution, potential aliasing, and quality of the array, respectively. Overall, the circular arrays with irregular station distribution are known as ideal arrays in which the resolution does not change with different azimuths (Rost and Tomas, 2002) and irregularity can account for spatial aliasing somewhat (Harmon *et al*., 2008). Although our array had not been designed for ambient noise surface wave studies, coherent informative signals can be recovered at some frequencies.

For beamforming analysis, the array aperture is large enough allowing maximum periods of ~20 seconds to resolve but due to frequency limits of the mid-band sensors, phases with maximum periods of 10 s can be emerged. For the best resolved frequencies (0.1-0.3 Hz) of the observational data, we derived coherent dispersive surface waves, and continuity of phase velocity estimations over most azimuths can be easily observed. Point sources contribution to the beamforming results, with different velocity estimations, does not distort continuity of the ring-shaped expected velocities. As shown in Fig. 3c, for 0.3 Hz frequency, point sources together with

the spatial aliasing may introduce some errors to the results while an average estimation of phase velocity distribution can be still extracted.

For cross-correlation technique, phase velocities are estimated from phase delay times between individual station pairs. Station pairs with distances shorter than 3 wavelengths are usually dropped mainly because of the far field approximation of the Green function interpretation (e.g. Bensen *et al*., 2007). Although our data are correlated in time domain, phase velocity estimations are based on the spectral method of the Bessel function which is applicable at shorter distances (Ekstrom *et al*., 2009). On the other hand, Menke and Jin (2015) reported that in small station distances the low number of zero-crossing points limits the resolution of interpolated dispersion curve. In our case, we deal with an average dispersion curve which is adequately approximated by all possible dispersion curves at different interstation spacing.

As shown in Fig. 5a, both of techniques yielded similar results and two average dispersion curves were almost overlapping within the error bars suggesting that reliable average phase velocities hold for estimation of good velocity model in this region. Some discrepancies in dispersion estimates are expected mainly because of the data quantity. Actually, the beamforming analysis is based on all data while cross-correlations come from good quality data, whereas some station pair correlations have been dropped during the process due to SNR criterion. Furthermore, high noise levels is the most significant limitation of the Bessel function method which can cause inaccurate determination of phase velocities where improbable sharp jumps in dispersion curve are detected (Menke and Jin, 2015). For this reason, we used SNR as a proxy to discriminate sufficiently high quality data sets for further analysis.

Up to now, there is no sufficient information of shallow velocity structure in this region. The available very near-surface information indicate that this region is a longitudinal asymmetrical valley filled by the alternation of gravel, sand, silt, and clay materials, and presence of thick alluvial deposits is documented in recent researches (Hafezi Moghaddas, 2008; Sajadian *et al*., 2015). The shear-wave model obtained in this study, reveals an average low velocity zone at 1 km upper layer which is consistent with thick alluvial deposits and other sediments. Low impedance and amplification effects of alluvial sediments can be responsible for large damages caused by earthquakes (e.g. Panza *et al*., 2000).

In summary, we have provided an average 1D shear-wave velocity model of the study area that not only can be directly used in early warning, risk mitigation, and environmental studies, but also as a good starting model to search for a 3D shallow velocity structure of this region.

Acknowledgements. We acknowledge data supports from the International Institute of Earthquake Engineering and Seismology (IIEES) for providing waveform data recorded by the temporary seismic network.

REFERENCES

Aki K.; 1957: *Space and time spectra of stationary waves with special reference to microtremors*. Bull. Earthquake Res. Inst. Univ. Tokyo, **35**, 415-456.

Alavi M.; 1992: *Thrust tectonics of the Binalood region, NE Iran*. Tectonics, **11**, 360-370, doi: 10.1029/91TC02217.

Ambraseys N. and Melville C.; 1982: *A history of Persian Earthquakes*. Cambridge Univ. Press, Cambridge, UK, 219 pp.

Bensen G.D., Ritzwoller M.H., Barmin M.P., Levshin A.L., Lin F., Moschetti M.P., Shapiro N.M. and Yang Y.; 2007: *Processing seismic ambient noise data to obtain reliable broad-band surface wave dispersion measurements*. Geophys. J. Int., **169**, 1239-1260, doi: 10.1111/j.1365-246X.2007.03374.

Boschi L., Weemstra C., Verbeke J., Ekstrom G., Zunino A. and Giardini D.; 2013: *On measuring surface wave phase velocity from station-station cross-correlation of ambient noise*. Geophys. J. Int., **192**, 346-358.

Bostenaru Dan M., Armas I. and Goretti A. (eds); 2014: *Earthquake hazard impact and urban planning*. Springer, Dordrecht, The Netherlands, 326 pp., doi: 10.1007/978-94-007-7981-5.

Ekstrom G., Abers G.A. and Webb S.C.; 2009: *Determination of surface-wave phase velocities across USArray from noise and Aki's spectral formulation*. Geophys. Res. Lett., **36**, L18301, doi: 10.1029/2009GL039131.

German A.P. and Beroza G.C.; 2008: *Earthquake ground motion prediction using the ambient seismic field*. Geophys. Res. Lett., **35**, L14304, doi: 10.1029/2008GL034428.

Gerstoft P. and Tanimoto T.; 2007: *A year of microseisms in southern California*. Geophys. Res. Lett., **34**, L20304, doi: 10.1029/2007GL031091.

Gerstoft P., Fehler M.C. and Sabra K.G.; 2006: *When Katrina hit California*. Geophys. Res. Lett., **33**, L17308, doi: 10.1029/2006GL027270.

Gouedard P., Cornou C. and Roux P.; 2008: *Phase-velocity dispersion curves and small-scale geophysics using noise correlation slantstack technique*. Geophys. J. Int., **172**, 971-981, doi: 10.1111/j.1365-1246X.2007.03654.x.

Hafezi Moghaddas N.; 2008: *Seismic microzonation of Mashhad city*. Khorasan Rzavi building and housing organization, Engineering geology report, vol. V, (in Persian).

Harmon N., Gerstoft P., Rychert C.A., Abers G.A., Salas de la Cruz M. and Fischer K.M.; 2008: *Phase velocities from seismic noise using beamforming and cross correlation in Costa Rica and Nicaragua*. Geophys. Res. Lett., **35**, L19303, doi: 10.1029/2008GL035387.

Herrmann R.B. and Ammon C.J.; 2002: *Computer programs in seismology-surface waves*. Receiver Functions and Crustal Structure, Saint Louis University, Saint Louis, MO, USA, <www.eas.slu.edu/People/RBHerrmann/ComputerPrograms.html>.

Hollingsworth J., Jackson J., Walker R., Gheitanchi M. and Bolourchi M.; 2006: *Strike-slip faulting, rotation, and along-strike elongation in the Kopeh Dagh Mountains, NE Iran*. Geophys. J. Int., **166**, 1161–1177.

Jackson J., Priestley K., Allen M. and Berberian M.; 2002: *Active tectonics of the south Caspian Basin*. Geophys. J. Int., **148**, 214-245, doi: 10.1046/ j.1365-246X.2002.01588.x.

Li H.Y., Su W., Wang C.Y. and Huang Z.X.; 2009: *Ambient noise Rayleigh wave tomography in western Sichuan and eastern Tibet*. Earth Planet. Sci. Lett., **282**, 201-211.

Lyberis N. and Manby G.; 1999: *Oblique to orthogonal convergence across the Turan block in the post-Miocene*. AAPG Bull., **83**, 1135-1160.

Masson F., Anvari M., Djamour Y., Walpersdorf A., Tavakoli F., Daignieres M., Nankali H. and Van Gorp S.; 2007: *Large-scale velocity field and strain tensor in Iran inferred from GPS measurements: new insight for the present-day deformation pattern within NE Iran*. Geophys. J. Int., **170,** 436-440, doi: 10.1111/j.1365-246X.2007.03477.x.

Menke W. and Jin G.; 2015: *Waveform fitting of cross spectra to determine phase velocity using Aki's formula*. Bull. Seismol. Soc. Am., **105**, 1619-1627.

Panza G.F., Romanelli F. and Vaccari F.; 2000: *Seismic wave propagation in laterally heterogeneous anelastic media: theory and applications to seismic zonation*. Adv. Geophys., **43**, 1-95.

Prieto G.A., Lawrence J.F. and Beroza G.C.; 2009: *Anelastic earth structure from the coherency of the ambient seismic field*. J. Geophys. Res., **114**, B07303, doi: 10.1029/2008JB006067.

Rost S. and Tomas C.; 2002: *Array seismology: methods and applications*. Rev. Geophys., **40**, 1008, doi: 10.1029/2000RG000100.

Sabra K.G., Gerstoft P., Roux P. and Kuperman W.A.; 2005: *Surface wave tomography from microseisms in Southern California*. Geophys. Res. Lett., **32**, L14311, doi: 10.1029/2005GL023155.

Sadeghisorkhani H., Gudmundsson O. and Tryggvason A.; 2018: *GSpecDisp: a matlab GUI package for phase-velocity dispersion measurements from ambient-noise correlations*. Comput. Geosci., **110**, 41–53.

Sajadian M.R., Pourkermani M., Qorashi M. and Hafezi Moghaddas N.; 2015: *The analysis of transverse topographic symmetry factor (T Index) in the Chekene-Mazavand. North east Iran*. Open J. Geol., **5**, 809-820, doi: 10.4236/ojg.2015.511069.

Sambridge M.; 1999: *Geophysical inversion with a neighborhood algorithm I*. Geophys. J. Int., **138**, 727-746.

Shabanian E., Siame L., Bellier O., Benedetti L. and Abbassi M.R.; 2009: *Quaternary slip rates along the northeast boundary of the Arabia-Eurasia collision zone (Kopeh Dagh Mountains, north-east Iran)*. Geophys. J. Int., **178**, 1055-1077, doi: 10.1111/j.1365-246X.2009.04183.x.

Shapiro N.M. and Campillo M.; 2004: *Emergence of broadband Rayleigh waves from correlations of the ambient seismic noise*. Geophys. Res. Lett., **31**, L07614, doi: 10.1029/2004GL019491.

Shapiro N.M., Campillo M., Stehly L. and Ritzwoller M.H.; 2005: *High resolution surface-wave tomography from ambient seismic noise*. Sci., **307**, 1615-1618.

Sherriff R.E. and Geldart L.P.; 1982: *Exploration seismology, I: history, theory, and data acquisition*. Cambridge Univ. Press, Cambridge, UK, 253 pp.

Stehly L., Campillo M. and Shapiro N.M.; 2006: *A study of the seismic noise from its long-range correlation properties*. J. Geophys. Res., **111**, B10306, doi: 10.1029/2005JB004237.

Stocklin J.; 1968: *Structural history and tectonics of Iran: a review*. AAPG Bull., **52**, 1229-1258.

Tavakoli F.; 2007: *Present-day kinematics of the Zagros and east of Iran faults*. PhD Thesis in Geophysics, University of Joseph Fourier, Grenoble, France, 314 pp.

Tchalenko J.S.; 1975: *Seismicity and structure of the Kopet Dagh (Iran, USSR)*. Philos. Trans. R. Soc. London, Ser. A, **278**, 1-28, doi: 10.1098/rsta.1975.0019.

Vernant P., Nilforoushan F., Hatzfeld D., Abbassi M.R., Vigny C., Masson F., Nankali H., Martinod J., Ashtiani A., Bayer R., Tavakoli F. and Chery J.; 2004: *Present-day crustal deformation and plate kinematics in the Middle East constrained by GPS measurements in Iran and northern Oman*. Geophys. J. Int., **157**, 381-398.

Wathelet M.; 2008: *An improved neighborhood algorithm: parameter conditions and dynamic scaling*. Geophys. Res. Lett., **35**, L09301, doi: 10.1029/2008GL033256.

Yao H. and van der Hilst R.D.; 2009: *Analysis of ambient noise energy distribution and phase velocity bias in ambient noise tomography with application to SE Tibet*. Geophys. J. Int., **179**, 1113–1132, doi: 10.1111/j.1365-246X.2009.04329.x.

Corresponding author: Seyyed Mahmood Azhari
Institute of Geophysics, University of Tehran
Amir Abad, Tehran14155-6466, Iran
Phone: +98 9155 614855; e-mail: azhari@ut.ac.ir